Research Article Vol. 59, No. 19 / 1 July 2020 / Applied Optics 5737

applied optics

Design of a panoramic annular lens with ultrawide angle and small blind area

KUN ZHANG,[1,2,3] XING ZHONG,[1,2,3,*] LEI ZHANG,[1,2,3] AND TIANQING ZHANG[1,2,3]

[1]Changchun Institute of Optics, Fine Mechanics and Physics, Chinese Academy of Sciences, Changchun 130033, China
[2]University of Chinese Academy of Sciences, Beijing 100049, China
[3]Chang Guang Satellite Technology Co., Ltd., Changchun 130102, China
*Corresponding author: ciomper@163.com

Received 21 April 2020; revised 28 May 2020; accepted 28 May 2020; posted 28 May 2020 (Doc. ID 395598); published 29 June 2020

A panoramic annular lens (PAL) comprises a panoramic annular head unit (PAHU) and a relay lens group. Due to the properties of annular imaging, single-channel PAL systems contain a blind area in the central field of view (FOV), which is difficult to reduce in a traditional optical system structure. Therefore, we propose a novel reflective PAHU structure, using two mirrors to replace the traditional single-lens- or multilens-cemented PAHU, to achieve a smaller blind area and ultrawide-angle imaging. In this paper, we present the design of an ultrawide-angle PAL with a FOV of (22° ~ 120°) × 360° using our proposed method. The resulting optical system achieves a blind area ratio of less than 3.67%. Compared with the traditional PAL system with the lowest blind area ratio, the blind area ratio of our system is reduced by half, demonstrating the feasibility of the proposed method.

https://doi.org/10.1364/AO.395598

1. INTRODUCTION

A direct-view panoramic annular lens (PAL) system can perform one-time imaging with a large field of view (FOV). Compared with scanning PAL systems, advantages of the direct-view PAL system include fast imaging speed, no mechanical moving parts, and strong anti-interference capabilities. There are two types of direct-view PAL system: First, the fisheye system, which uses a central projection method; this system has the disadvantages of significant distortion and complex structure and is not conducive to miniaturization; second, the PAL system with planar cylindrical projection, which has the advantages of low distortion, compact structure, and larger FOV compared with the fish eye system. The PAL system has therefore become a hot research topic in recent decades [1–3], finding wide application in areas such as machine vision, security monitoring, atmospheric monitoring, space flight navigation, and pipeline inner wall detection [4].

A single-channel PAL system is composed of two parts: The panoramic annular head unit (PAHU) and the relay lens group. The PAHU is a catadioptric structure composed of a single lens or multiple-cemented lenses [5,6]. Due to the characteristics of annular imaging, there is inevitably a central blind area in the PAL system. Therefore, global research has focused on obtaining a small blind area and large FOV [7,8]. Using a single-lens PAHU structure, Wang *et al.* designed a PAL with an f-number of 5 and an FOV of (55° ~ 115°) × 360° [9]. Using a three-lens-cemented PAHU structure, Huang *et al.* designed a PAL with an FOV of (30° ~ 100°) × 360° [10]. Cheng *et al.* employed an annularly stitched aspherical surface to design a PAL with an FOV of (90° ~ 135°) × 360° [11]. Using a single-lens PAHU structure and three Q_{bsf} aspheric surfaces, Zhou *et al.* designed a PAL with an FOV of (30° ~ 120°) × 360° [12], as shown in Fig. 1, where S_{12}, S_{13}, and S_{14} are three Q_{bsf} aspheric surfaces.

Single-channel PAL systems generally use a catadioptric PAHU structure. In a PAL system, the single-lens- or multilens-cemented PAHU needs to refract and reflect the incident light multiple times [13,14], so the system design must consider occlusion of imaging light. This requirement makes it difficult to further reduce the blind area in the central FOV using a traditional optical system structure [15,16]. In addition, the larger the PAL system's FOV, the larger the diameter of the PAHU. This results in a heavy single-lens- or multilens-cemented PAHU, which makes it difficult to achieve a lightweight design.

In this paper, we propose a new design method based on a reflective PAHU structure to address the above shortcomings. Our PAHU design employs two mirrors, with the incident light reflected only twice, achieving a simplified optical path. Using this method, we designed a PAL with a FOV of (22° ~ 120°) × 360°. Our results show that the reflective PAL not only achieves a large FOV but also significantly reduces the blind zone ratio of the central FOV and improves detector utilization. Furthermore, the system is light and compact.

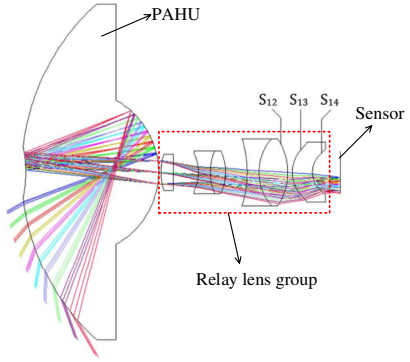

Fig. 1. Structure of the catadioptric PAL system [12].

2. PAL SYSTEM DESIGN PRINCIPLES

A. PAHU Structure Selection

PAL systems are large FOV optical systems, in which field curvature is an important factor in determining imaging quality and must therefore be carefully constrained. According to Seidel aberration theory, field curvature is determined by the fourth Seidel factor, known as the Petzval sum [17], as shown in Eq. (1):

$$P = J^2 \sum_{i=1}^{n} \frac{\phi_i}{n_i}, \tag{1}$$

where J is the Lagrange invariant, ϕ_i is the optical power of the ith lens, and n_i is the refractive index of the ith lens.

In Seidel aberration theory, an optical system with good field curvature correction should satisfy the requirement represented by Eq. (2):

$$P = J^2 \sum_{i=1}^{n} \frac{\phi_i}{n_i} = 0. \tag{2}$$

However, the PAL's relay lens group often has a positive optical power, resulting in a positive Petzval sum, so the Petzval sum of the PAHU needs to be less than zero. The PAHU's Petzval sum can be evaluated with Eq. (3):

$$P = \sum_{i=1}^{n} P_i = J^2 \sum_{i=1}^{n} \frac{n_i' - n_i}{n_i' n_i} c_i, \tag{3}$$

where n_i and n_i' are the refractive indices before and after the ith surface, respectively. When the ith surface is a reflective surface, $n_i' = -n_i$.

In this paper, the PAHU is composed of only two mirrors. According to Eq. (3), the Petzval sum of the PAHU can be calculated by Eq. (4):

$$P_1 = J^2 \sum_{i=1}^{2} \frac{n_i' - n_i}{n_i' n_i} c_i = 2J^2(c_1 - c_2), \tag{4}$$

where c_1 and c_2 are the curvature of the primary and secondary mirrors, respectively.

From Eq. (4), we can see that, if the PAHU's Petzval sum is negative, $(c_1 - c_2) < 0$ must be guaranteed.

In this paper, we propose a PAHU design that uses two mirrors. There are only two types of mirror: convex and concave.

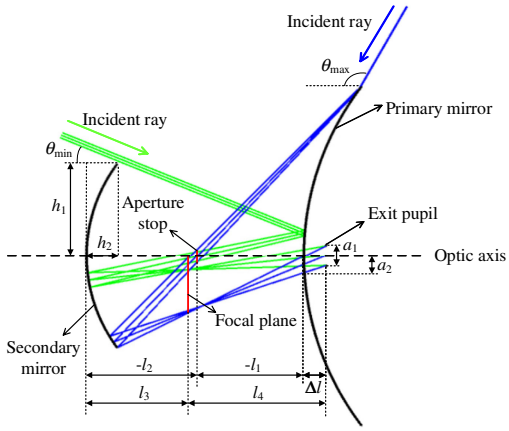

Fig. 2. Imaging principle diagram of the PAHU.

For the primary mirror to achieve normal reflection of incident light greater than 90°, it can only be a convex mirror; thus, the curvature of the primary and secondary mirrors should meet the requirements of Eq. (5):

$$c_2 > c_1 > 0. \tag{5}$$

Secondary imaging can compress the PAHU's aperture to make the PAL more compact. A PAL system with an aperture stop between the PAHU and the relay lens group can better eliminate stray light [10,18]. The imaging principle of the PAHU is as shown in Fig. 2. Incident light is first reflected by the primary mirror and then reflected by the secondary mirror for the first imaging; further, the aperture stop is located between the primary mirror and the secondary mirror. The aperture stop here is just the PAHU's aperture stop, owing to the PAHU is only a part of the PAL, so the PAL's mechanical aperture stop is placed at the exit pupil of the PAHU practically.

B. Calculation Method for Blind Area and Initial Structure

Selecting a suitable exit pupil position for the PAHU is essential. The exit pupil not only needs to match the entrance pupil of the relay lens group but is also closely related to the size of the blind area in the central FOV. A traditional two-reflection optical system generally places the aperture stop at the primary or secondary mirror, but that approach is not suitable here. To minimize the blind area, it is necessary to properly control the distance between the primary and secondary mirrors and to reduce the height of the PAHU's outgoing light on the primary mirror. Hence, the exit pupil position should ideally coincide with the position of the primary mirror. However, to facilitate practical assembly, we placed the exit pupil on the right side of the primary mirror to obtain Eq. (6):

$$\Delta l = l_3 + l_4 - l_1 - l_2, \tag{6}$$

where l_1 is the distance between the primary mirror and the aperture stop, l_2 is the distance between the aperture stop and the secondary mirror, l_3 is the distance between the secondary mirror and the focal plane, and l_4 is the distance between the focal plane and the exit pupil.

The PAL system's blind area is caused by two major factors: One is the occlusion of the secondary mirror to the incident light; the other is the maximum height of the PAHU's outgoing light on the primary mirror. The greater the maximum height, the greater the blind area. This can be addressed by placing the PAHU's exit pupil close to the primary mirror. Let us perform a theoretical analysis of the first factor.

The rise equation for the secondary mirror is

$$h_2 = r_2 - \sqrt{{r_2}^2 - {h_1}^2}, \tag{7}$$

where r_2 is the radius of the secondary mirror, and h_1 is the half aperture of the secondary mirror.

The maximum height of the PAHU's outgoing light on the primary mirror is

$$a_2 = \Delta l \times |\beta_I| \times \tan(\theta_{\max}) + \frac{a_1}{2}, \tag{8}$$

where β_I is the angular magnification of the PAHU, $\theta_{\max}$ is the maximum FOV of the PAHU, and a_1 is the exit pupil diameter of the PAHU.

From Eqs. (7) and (8), we can calculate the minimum FOV of the PAL system with Eq. (9):

$$\tan(\theta_{\min}) = \frac{h_1 - \Delta l \times |\beta_I| \times \tan(\theta_{\max}) + \frac{a_1}{2}}{l_1 + l_2 - r_2 + \sqrt{{r_2}^2 - {h_1}^2}}. \tag{9}$$

The blind area ratio represents the ratio of the blind area to the total area on the focal plane. The blind area ratio of the PAL can be calculated with Eq. (10):

$$\eta = \frac{\pi (f\theta_{\min})^2}{\pi (f\theta_{\max})^2} \times 100\% = \left(\frac{\theta_{\min}}{\theta_{\max}}\right)^2 \times 100\%, \tag{10}$$

where f is the total focal length of the PAL.

As can be seen from Fig. 2, the aperture stop is located at the exit pupil after imaging by the secondary mirror. Using the mirror's imaging principle, we can obtain Eq. (11):

$$\frac{1}{l_2} + \frac{1}{l_3 + l_4} = \frac{2}{r_2}. \tag{11}$$

The incident light is imaged on the focal plane after being reflected by the primary mirror and the secondary mirror. Using the imaging principle, we obtain Eq. (12):

$$\frac{2}{2l_1 + 2l_2 + r_1} + \frac{1}{l_3} = \frac{2}{r_2}, \tag{12}$$

where r_1 is the radius of the primary mirror.

The PAHU's total focal length is the focal length of the primary mirror multiplied by the magnification of the secondary mirror:

$$f_I = \beta_2 f_a = \frac{r_1 l_3}{2l_1 + 2l_2 + r_1}, \tag{13}$$

where f_I is the focal length of the PAHU, β_2 is the magnification of the secondary mirror, and f_a is the focal length of the primary mirror.

The structural parameters of the PAHU cannot be directly solved by Eqs. (5)–(13), so the assignment method can be used to calculate the parameters and focal length.

The relay lens group not only performs secondary imaging in the PAL system but also compensates for the PAHU's residual aberrations. The PAL system's total focal length can be calculated based on the focal length of the PAHU and the magnification of the relay lens group, as shown in Eq. (14):

$$f = \beta_{II} f_I, \tag{14}$$

where β_{II} is the magnification of the relay lens group.

3. PAL DESIGN PROCESS

A. Design Parameters

To achieve better imaging performance in the optical system, the detector and the optical lens should be matched. Therefore, it is necessary to select a reasonable detector before designing the optical system. The detector's pixel size is closely related to image signal-to-noise ratio (SNR) and resolution. A larger pixel size will provide better SNR but reduced resolution. Taking the focal length and FOV of the PAL into consideration, we selected a detector pixel size of 5 μm × 5 μm and a Nyquist frequency of 100 lp/mm.

Since the half FOV of an ultrawide-angle PAL system is greater than 90°, the normal projection relationship between object and image cannot be applied; thus, the corresponding relationship between object and image is the F-theta projection. Ultrawide-angle PAL systems generally have large relative distortion, causing stronger image compression at the edge of the

Table 1. PAL System Design Parameters

Parameter	Value
Working spectrum	486–656 nm
Effective focal length	2.0 mm
f-number	4
FOV	(22° × 120°) × 360°
F-theta distortion	<4%

Table 2. Initial Structural Parameters of the PAHU

l_1/mm	l_2/mm	l_3/mm	l_4/mm	r_1/mm	r_2/mm
9	10	8.7	12.35	24.5	13.6

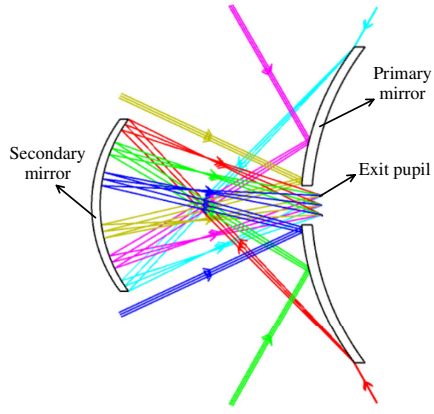

Fig. 3. Structure of the PAHU.

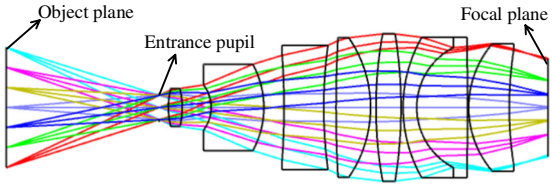

Fig. 4. Structural diagram of the relay lens group.

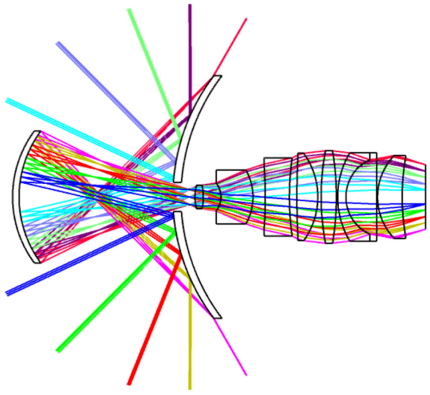

Fig. 5. Structure of the PAL.

FOV, which is highly unfavorable for information acquisition. Hence, the optical system's relative distortion must be minimized. After careful consideration, the major design parameters for our ultrawide-angle PAL system were selected as presented in Table 1.

B. Design of the PAHU

The number of unknown parameters in Eqs. (5)–(13) is greater than the number of equations, so the assignment method can be used to calculate the structural parameters, which can then be used in optical design software for optimization. The magnification empirical value of the relay lens group of the PAL can be selected from 0.5 to 0.7, which can correct the aberrations of the PAL better. The calculated initial structural parameters of the PAHU are shown in Table 2.

After calculation, the parameters in Table 2 were used in the optical design software for preliminary optimization. In the optimization process, the distance between primary and secondary mirrors must be properly controlled to reduce the blind area in the central FOV. The structure of the optimized PAHU is shown in Fig. 3.

C. Relay Lens Group Design

When designing a PAL system, the relay lens group is important to secondary imaging and aberration correction. The PAHU needs to provide the primary image, but it also has a large FOV, with few variables suitable for optimization, so it will inevitably cause large residual aberrations. To achieve good imaging quality, these residual aberrations need to be compensated for by the relay lens group. To meet the matching requirement between the PAHU and the relay lens group, the PAHU's exit pupil position should be the same as the relay lens group's entrance pupil position. We optimize a classical structure to a specific magnification calculated by Eq. (14) as the relay lens group. The object height of the relay lens group is the image height of the PAHU. Figure 4 shows a structural diagram of the relay lens group.

The PAHU and relay lens group designs were combined and optimized in optical design software. In the optimization process, we first had to control the optical system's relative distortion and then improve imaging quality. The structure of the PAL is shown in Fig. 5.

D. Relative Illumination Optimization

Relative illumination is the ratio of the irradiance of the off-axis FOV on the focal plane to the irradiance of the center FOV of the focal plane after the object light passes through the optical system. After an ideal lens images to a uniform light field, the relative illumination of the off-axis FOV on the focal plane decreases with the law of the cosine fourth power.

Add the operand RELI to the merit function of the optical design software and then optimize the PAL to increase the relative illumination. Figure 6 shows the relative illumination curve

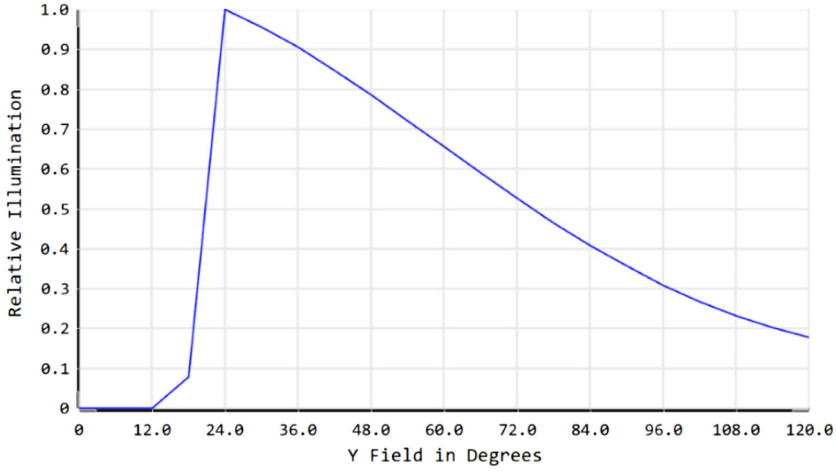

Fig. 6. Relative illumination of the PAL.

Table 3. Structural Parameters of the PAHU

Mirror	Radius/mm	Conic	a_2	a_4	a_6
Primary mirror	25.3	−0.569	0	−08.755e-6	0
Secondary mirror	12.9	−00.207	0	−02.068e-5	0

of the PAL system. It can be seen that relative illumination of the full FOV drops quickly and, at 120°, is less than 0.2, which does not meet the usage requirements.

In actual optical systems, relative illumination is affected by vignetting, pupil aberration, and distortion. In large FOV optical systems such as PAL systems, the presence of pupil spherical aberration often results in the diameter of the off-axis entrance pupil being larger than that of the on-axis entrance pupil. Therefore, the light energy entering the optical system from the off-axis FOV is greater than that from the on-axis FOV, and the off-axis relative illumination no longer decreases with the law of the cosine fourth power [11]. In addition, if the optical system is designed as an image space telecentric system, the change of relative illumination on the focal plane will be reduced.

The PAL system designed in this paper has strict distortion requirements, so we cannot increase relative illumination by increasing distortion. Setting vignetting to improve relative illumination is also undesirable in this optical system, so the only feasible option is to use pupil spherical aberration to make the diameter of the off-axis entrance pupil larger than that of the on-axis entrance pupil.

To improve relative illumination, it is necessary to increase the PAHU's low number of variables by using the pupil spherical aberration of the optical system. However, even aspheric surfaces are easy to process, employ mature technology, and are widely used. The equation for an even aspheric surface is Eq. (15):

$$z = \frac{cr^2}{1+\sqrt{1-(1+k)\cdot c^2 r^2}} + \sum_{m=0}^{M} a_{2m+2} r^{2m+2}, \tag{15}$$

where r is the height of light passing through the lens surface, c is the curvature at the vertex of the aspheric surface, $k = -e^2$ is the conic coefficient of the quadric surface, and a_{2m+2} is the coefficient of the even aspheric surface.

In the optical design software, after changing the primary and the secondary mirrors to be even aspheric surfaces, we first optimized the PAHU, followed by the relay lens group, before performing overall optimization of the optical system. Table 3 shows the parameters of the primary and secondary mirrors in the optimized PAHU. Figure 7 shows the relative illumination of the optimized PAL system. From Fig. 7, it can be seen that the relative illumination of the full FOV is greater than 0.65 and drops slowly. Our design results demonstrate the feasibility of our method of improving relative illumination by increasing the diameter of the off-axis entrance pupil.

The structure of the PAL after increasing relative illumination is shown in Fig. 8. As can been seen from Fig. 8 that when the imaging point gets closer to the central FOV, the tangential magnification will become smaller than the radial magnification. This phenomenon is determined by the F-theta projection. The maximum image height of the central blind area is 0.77 mm, and the image height of the maximum imaging area is 4.02 mm, so the blind area rate is less than 3.67%. Due to the distortion of the PAL, the blind area ratio here is slightly different from the value calculated by Eq. (10).

4. PAL DESIGN RESULTS

A. Image Quality Evaluation

Spot diagrams, modulation transfer functions (MTF), and distortion are important indicators for evaluating image quality in optical systems. Each point in the spot diagram corresponds to a ray, and the size of the diffuse spot depends entirely on the position of each ray on the focal plane; thus, it can be used to accurately judge the diffusion of the imaging light in the optical system. The smaller the root mean square (RMS) radius of the diffuse spot, the better the imaging quality of the optical system. Figure 9 shows the PAL's spot diagram, in which the circles represent the diffraction limit of each FOV. It can be seen from Fig. 9 that the RMS radius of the PAL's full FOV is close to the diffraction limit.

The imaging performance of the optical system can be comprehensively evaluated with an MTF that represents the change law of the image's modulation degree. Figure 10 shows the PAL

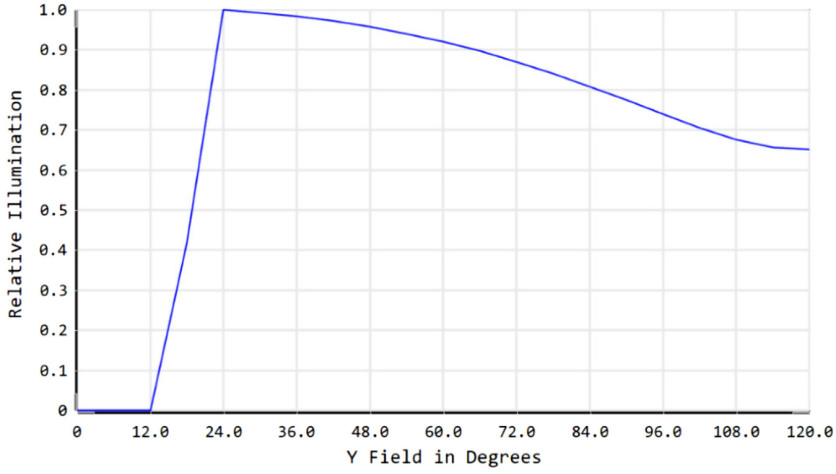

Fig. 7. Relative illumination curve of the optimized PAL system.

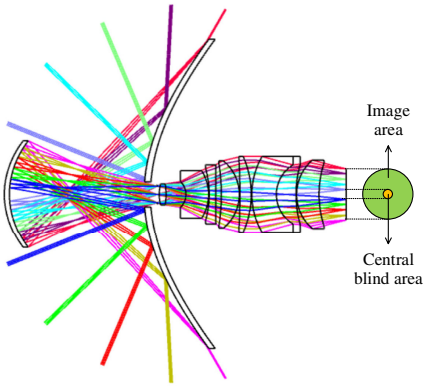

Fig. 8. Structure of the optimized PAL.

system's MTF curve. It can be seen that the MTF of the PAL system's full FOV at the Nyquist frequency of 100 lp/mm is greater than 0.35, so the optical system has good imaging quality.

The half FOV of the ultrawide-angle PAL system designed in this paper is 120°, so the relationship between object and image is the F-theta projection. Figure 11 shows the PAL system's field curvature and distortion diagram. It can be seen that the maximum distortion of the PAL system is less than 4%.

B. Tolerance Analysis

It is important to perform tolerance analysis before mass production of the lens. Using the optical design software's MTF tolerance analysis function, the lens manufacturing difficulty can be evaluated. In the tolerance analysis, the MTF of the

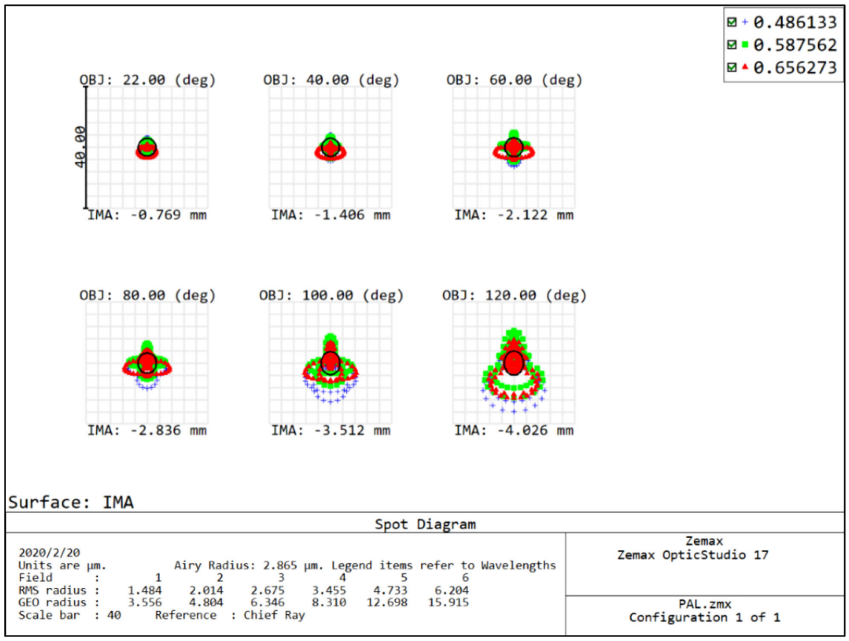

Fig. 9. Spot diagram.

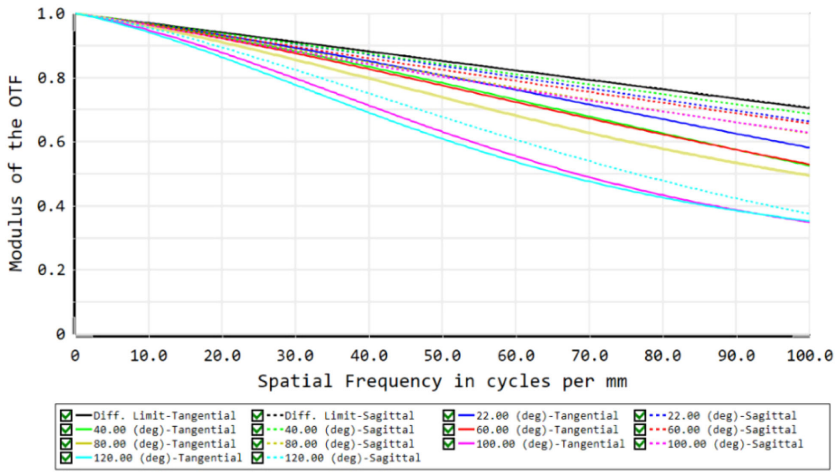

Fig. 10. MTF diagram of the PAL.

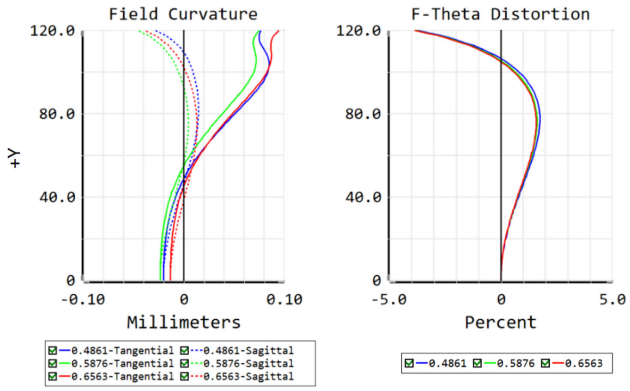

Fig. 11. Field curve and distortion diagram.

Table 4. Tolerance Distribution of the PAL

Tolerance Items	Value
Radius (fringe)	≤3
Thickness (mm)	±0.02
Surface decenter (mm)	±0.02
Element tilt (°)	±0.02
Element decenter (mm)	±0.02
Surface irregularity (fringe)	≤0.3
Refractive index	±0.001
Abbe number (%)	±0.5

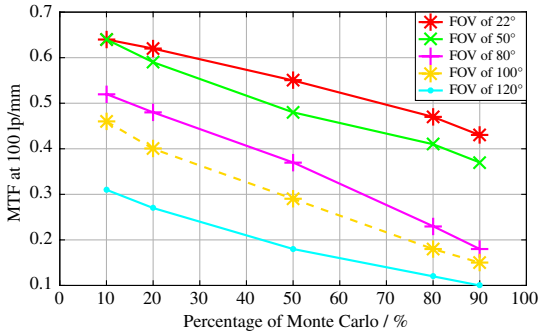

Fig. 12. Monte Carlo analysis chart.

Nyquist frequency of 100 lp/mm is used as the merit function. First, inverse sensitivity analysis is performed on the PAL. Then, the approximate range of each manufacture and assembly tolerance of the PAL can be obtained. Second, the obtained tolerance range is set to carry out sensitivity analysis, and the sensitive tolerance need to be restricted. Finally, the rationality of the tolerance is evaluated by Monte Carlo simulation. Table 4 presents the tolerance distribution table for the ultrawide-angle PAL system. The PAL's MTF at Nyquist frequency of 100 lp/mm is shown in Fig. 12.

C. Mechanical Structure

In a coaxial two-reflection optical system, the standard approach is to use a metal bracket to connect the primary and secondary mirrors. Since the thermal expansion coefficient of the metal is close to that of the glass material, when the environmental temperature changes, the distance between the primary mirror and secondary mirror connected by the metal bracket changes little. Generally, the imaging quality of the optical system can be better guaranteed after athermal design. The PALs in [9,19] are both connected by a metal bracket, so the PAL designed in this paper also adopts this kind of mechanical structure. As shown in Fig. 13, the secondary mirror is assembled with three metal brackets, and the imaging light enters the PAL through the gaps between the metal brackets.

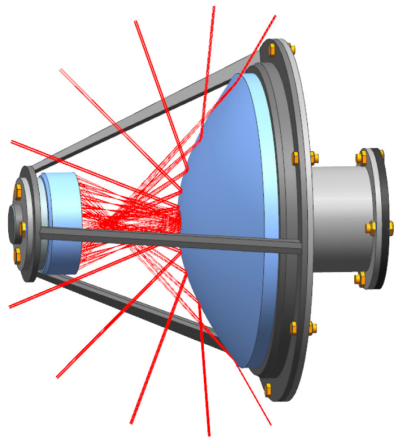

Fig. 13. Mechanical structure of the PAL.

5. CONCLUSION

In PAL systems, annular imaging characteristics result in generation of a central blind area, which is difficult to reduce in traditional single-channel PAL systems. Therefore, researchers have gradually turned their attention toward dual-channel PAL systems. In this paper, we propose a new method for designing a single-channel PAL system. Compared with the traditional approach, the PAL system designed using our method has a smaller blind area ratio and ultrawide angle. First, we proposed use of two mirrors to replace the traditional PAHU and analyzed the imaging principle of the PAHU. Second, we used that mathematical model to design the PAHU and relay lens group. Finally, we improved the relative illumination and imaging performance of the PAL system and designed an ultrawide-angle PAL with a focal length of −2.0 mm, f-number of 4, and FOV of $(22° \sim 120°) \times 360°$. The resulting design demonstrates a PAL with a reduced blind area ratio of less than 3.67%, low distortion, and good relative illumination and imaging quality. Additionally, the optical system is compact. The PAL can be used in applications, including machine vision, security monitoring, and pipeline inner wall detection.

Disclosures. The authors declare no conflicts of interest.

REFERENCES

1. G. Kweon, K. T. Kim, G. Kim, and H. Kim, "Folded catadioptric panoramic lens with an equidistance projection scheme," Appl. Opt. **44**, 2759–2767 (2005).

2. X. J. Li, D. W. Feng, and Y. Xiang, "Refractive-diffractive hybrid panoramic annular optical system," Laser Optoelectron. Prog. **56**, 232–237 (2019).
3. H. Q. Wu, X. Y. Zeng, and P. Wang, "Design of catadioptric IR panoramic imaging optical system," Infrared **40**, 1–6 +35 (2019).
4. X. D. Zhou, "Super-wide angle high-resolution panoramic annular lens design," Ph.D. thesis (Zhejiang University, 2016).
5. G. I. Kweon, K. Kim, Y. H. Choi, G. Kim, H. Kim, and S. Yang, "A catadioptric double-panoramic lens with the equidistance projection for a rangefinder application," Proc. SPIE **5613**, 29–42 (2004).
6. T. Ma, J. C. Yu, P. Liang, and C. H. Wang, "Design of a freeform varifocal panoramic optical system with specified annular center of field of view," Opt. Express **19**, 3843–3853 (2011).
7. W. M. Li and Y. F. Li, "Single-camera panoramic stereo imaging system with a fisheye lens and a convex mirror," Opt. Express **19**, 5855–5867 (2011).
8. D. Hui, M. Zhang, Z. Geng, Y. F. Zhang, J. Y. Duan, A. C. Shi, L. Hui, Q. Fang, and Y. L. Liu, "Designs for high performance PAL-based imaging systems," Appl. Opt. **51**, 5310–5317 (2012).
9. X. H. Wang, X. Zhong, R. F. Zhu, F. Gao, and Z. Q. Li, "Extremely wide-angle lens with transmissive and catadioptric integration," Appl. Opt. **58**, 4381–4389 (2019).
10. Z. Huang, J. Bai, T. X. Lu, and X. Y. Hou, "Stray light analysis and suppression of panoramic annular lens," Opt. Express **21**, 10810–10820 (2013).
11. D. W. Cheng, C. Gong, C. Xu, and Y. T. Wang, "Design of an ultrawide angle catadioptric lens with an annularly stitched aspherical surface," Opt. Express **24**, 2664–2677 (2016).
12. Y. H. Huang, Z. Y. Liu, Y. G. Fu, and H. Zhang, "Design of a compact two-channel panoramic optical system," Opt. Express **25**, 27691–27705 (2017).
13. Y. J. Luo, X. Huang, J. Bai, and R. G. Liang, "Compact polarization-based dual-view panoramic lens," Appl. Opt. **56**, 6283–6287 (2017).
14. Z. Huang, J. Bai, and X. Y. Hou, "Design of panoramic stereo imaging with single optical system," Opt. Express **20**, 6085–6096 (2012).
15. J. H. Wang, Y. C. Liang, and M. Xu, "Design of panoramic lens based on ogive and aspheric surface," Opt. Express **23**, 19489–19499 (2015).
16. L. Jiang, W. Huang, and W. C. Xu, "Panoramic lens for full view monitoring," J. Appl. Opt. **33**, 1–4 (2012).
17. X. D. Zhou, J. Bai, C. Wang, X. Y. Hou, and K. W. Wang, "Comparison of two panoramic front unit arrangements in design of a super wide angle panoramic annular lens," Appl. Opt. **55**, 3219–3225 (2016).
18. T. X. Lu, J. Bai, Z. Huang, and K. W. Wang, "Stray light analysis and suppression of panoramic annular lens," Acta Opt. Sinica **33**, 104–112 (2013).
19. J. H. Jo, S. Lee, H. J. Seo, J. H. Lee, and J. M. Kim, "Design of omnidirectional camera lens system with catadioptic system," Proc. SPIE **8788**, 87882Q (2013).